

Article

Effect of Drying–Wetting Cycle and Vibration on Strength Properties of Granite Residual Soil

Jiarun Tang and Dongxia Chen *

Department of Civil Engineering, Xiamen University, Xiamen 361005, China

* Correspondence: dongxiachen@xmu.edu.cn

Abstract: Granite residual soil (GRS) exhibits favorable engineering properties in its natural state. However, a hot and rainy climate, combined with vibrations generated during mechanical construction, can cause a notable decrease in its strength. In this study, the evolution of stress–strain curves and strength parameters (cohesion c and internal friction angle φ), unconfined compression strength (UCS) under drying and wetting (DW) cycles and vibration were investigated by means of direct shear test and UCS test. Furthermore, modified formulas for calculating shear strength and UCS under DW cycles and vibration were proposed, and their accuracy was verified. The results are as follows: The stress–strain curve of shear strength exhibits strain-hardening characteristics, and the shear compressibility of the sample increases with the number of DW cycles and vibration time. However, the stress–strain curve of UCS shows strain-softening properties, and the peak strength shifts forward with the number of DW cycles and vibrations. With the increase in the number of DW cycles and the vibration time, c shows a non-linear degradation, with a maximum degradation of 58.6%. φ fluctuates and increases due to the densification effect of DW cycles, but the influence of vibration on φ decreases with the increase in the number of DW cycles. UCS rapidly decreases and gradually stabilizes after DW cycles and vibration, with a maximum degradation of 81.1%. This study can serve as a reference for the stability analysis of GRS pits subjected to long-term influences of hot and rainy climates and mechanical vibration, providing valuable insights for future research.

Keywords: granite residual soil; drying–wetting cycle; vibration; strength deterioration



Citation: Tang, J.; Chen, D. Effect of Drying–Wetting Cycle and Vibration on Strength Properties of Granite Residual Soil. *Appl. Sci.* **2024**, *14*, 458. <https://doi.org/10.3390/app14010458>

Academic Editor: Asterios Bakolas

Received: 7 December 2023

Revised: 29 December 2023

Accepted: 31 December 2023

Published: 4 January 2024



Copyright: © 2024 by the authors. Licensee MDPI, Basel, Switzerland. This article is an open access article distributed under the terms and conditions of the Creative Commons Attribution (CC BY) license (<https://creativecommons.org/licenses/by/4.0/>).

1. Introduction

Granite residual soil (GRS) is a prevalent regional soil in southeast China, characterized by variations in weathering types and mineral components due to climatic differences [1]. The main mineralogical components of GRS in Xiamen, Fujian Province, are quartz, kaolinite, illite and small amounts of hematite [2–4]. The specific engineering properties of GRS are determined via its mineral compositions and structural properties. While the natural state of GRS exhibits high strength and low compressibility, it is prone to softening and disintegration when exposed to water [5–7]. These deterioration characteristics pose threats to the safety of geotechnical engineering projects, such as tunnel construction, highway subgrade construction and foundation pit excavation [8,9].

The distribution areas of GRS are primarily located in subtropical monsoon regions with hot and rainy summers, resulting in a constant process of drying and wetting that leads to changes in its macro-mechanical behavior and microstructural characteristics. Numerous studies have examined the degradation of the engineering properties of GRS caused by drying–wetting (DW) cycles. The impact of DW cycles on the macroscopic mechanical behavior of GRS has been investigated [10–12]. For instance, Jian et al. [13] found that the cohesion of GRS decreased significantly during the early stages of DW cycles, then gradually stabilized over time, while the internal friction angle did not exhibit a clear change. Similarly, Yu et al. [14] reached similar conclusions. Liu et al. [15] conducted 15 triaxial tests and found that the contact between fine particles was enhanced due to

the effects of DW cycles, resulting in an increase in cohesion with the number of DW cycles. After four DW cycles, the cohesion doubled while the internal friction angle slightly decreased. The mechanical properties of GRS are closely related to changes in microstructure and cracks [4]. Several studies have analyzed the effects of DW cycles on the macro-mechanical behaviors from the changes in microstructure and cracks. Liu et al. [16] investigated the correlation among the development of cracks, shear strength degradation and DW cycles in GRS and proposed a calculation formula for crack depth and strength degradation. An et al. [17] found that exponential decreases in effective cohesion and effective internal friction angle occur with the increase in the number of DW cycles, using triaxial consolidation undrained tests. With the help of computer tomography, nuclear magnetic resonance and scanning electron microscopy it was demonstrated that the fracture evolution and a transition in particle and pore structure led to fatigue damage of soil structure, resulting in the attenuation of the mechanical properties of GRS.

The mechanical properties of GRS are also significantly affected by mechanical vibrations during subway and tunnel construction [18–22]. Indoor tests of simulating soil sample disturbance mainly use sample vibration and sample extrusion. Since a vibration test can quantitatively control parameters such as vibration time, this method is more used for disturbance research. Commonly used vibration methods include the shaking table [23,24], the GDS dynamic triaxial instrument [25,26] and the vibrating sieve machine [27,28]. These methods destroy the original structure between soil particles through vibration and obtain disturbed samples. Currently, the research on vibration affecting the mechanical and compression properties of soils mainly focuses on silt clays and soft clays. Deng et al. [23] simulated the disturbance of soft soil using an indoor shaking table and determined that the unconfined compression strength (UCS) decreases with increasing vibration time. Additionally, the slope of the consolidation compression curve increases before yielding. Liu et al. [29] investigated the impact of vibration on the thixotropic strength recovery of silt. They found that, at the same frequency and rate, longer vibration times result in greater disturbance. The absolute strength recovery of silt was positively correlated with its disturbance degree, while its relative strength recovery was negatively correlated under the same static time. Based on this research, Liu et al. [30] examined the effect of different water contents on the strength recovery of disturbed silt. When the soil is vibrated for the same duration, the degree of disturbance is positively correlated with the water content, and the strength recovery is negatively correlated with water content. Liu et al. [31] employed dynamic and static triaxial instruments to investigate the changes in static shear strength of silty clay under different vibration loads, perimeter pressures and overconsolidation ratios. The results indicated that the specimen behaved similarly to the overconsolidated soil under vibration loads. When the similar over-consolidation ratio (SOCR) was less than 1.25, vibration had a minimal effect on the shear strength. However, when the SOCR exceeded 1.25, the shear strength rapidly decreased.

In summary, the impact of DW cycles on GRS has been thoroughly investigated from macroscopic to mesoscopic to microscopic levels. However, the research on the effects of vibration on GRS is still inadequate, and studies on the combined influence of both factors are exceedingly rare. Nevertheless, under the interaction between DW cycles and vibrations, GRS will undergo multi-field coupling and discrete damage processes, resulting in a complex deterioration process of its strength characteristics. Consequently, this work focuses on the strength characteristics of GRS under DW cycles and vibrations. DW cycle tests and vibration tests are conducted to simulate the effects of hot and rainy climates as well as mechanical vibration on GRS. Straight shear tests and UCS tests are utilized to explore the effect of DW cycles and vibrations on the strength characteristics of GRS. Based on these tests, the aim of the present research is to contribute more reliable calculation results when applied to the stability analysis of GRS foundations affected by hot and rainy weather and mechanical vibration.

2. Experimental Setup

2.1. Test Materials

GRS from a foundation pit in the Xiamen Metro Line 3 was used as the test soil in this study. It was obtained through open excavation at a depth ranging from 5 m to 6 m. Samples were taken from the site, and remolded specimens were prepared in the laboratory (Figure 1).

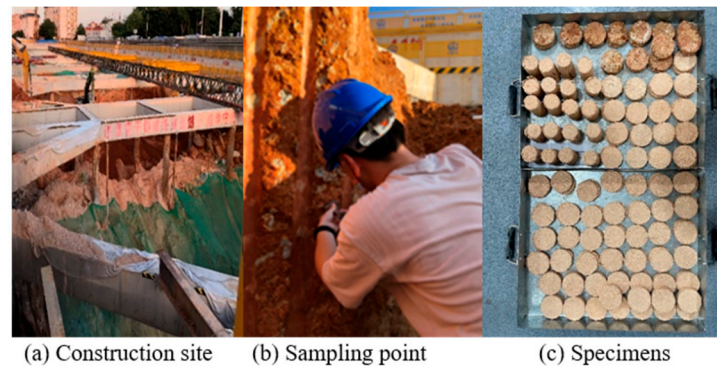


Figure 1. Sample taken on site and made.

According to the specification Standard for Geotechnical Testing Method (GB/T 50123-2019) [32], the physical and mechanical properties and the particle grading of GRS were measured, and the results are shown in Table 1 and Figure 2. The soil sample composition is mainly composed of gravel (19.2%), sand (72.7%) and fine particles (8.1%). According to the design code for building foundations (DBJ/T-15-31-2016) [33], when the gravel content does not exceed 20% of the total mass, it is considered sandy clay, so the soil used in this experiment is classified as residual sandy clay.

Table 1. Physical and mechanical properties of GRS.

Natural Density $\rho/g\cdot cm^{-3}$	Water Content $w/\%$	Dry Density $\rho_d/g\cdot cm^{-3}$	Specific Gravity G_s	Liquid Limit $LL/\%$	Plastic Limit $PL/\%$	Plasticity Index $PI/\%$	Void Ratio e
2.01	17.4	1.71	2.72	31.92	18.83	13.09	0.58

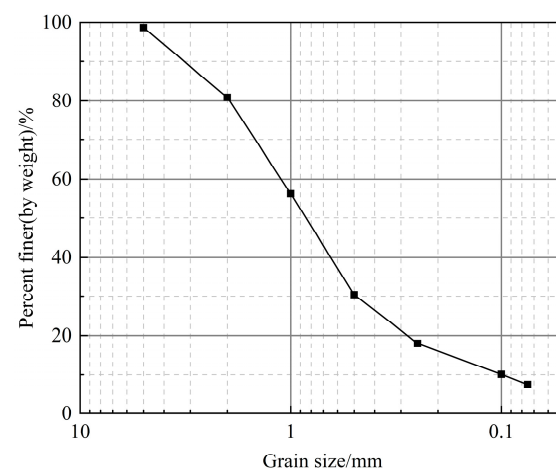


Figure 2. Grain size distribution curve of GRS.

2.2. Test Methods

The experiment consists of sample preparation, vibration simulation, DW cycle process and mechanical test. A flowchart is shown in Figure 3.

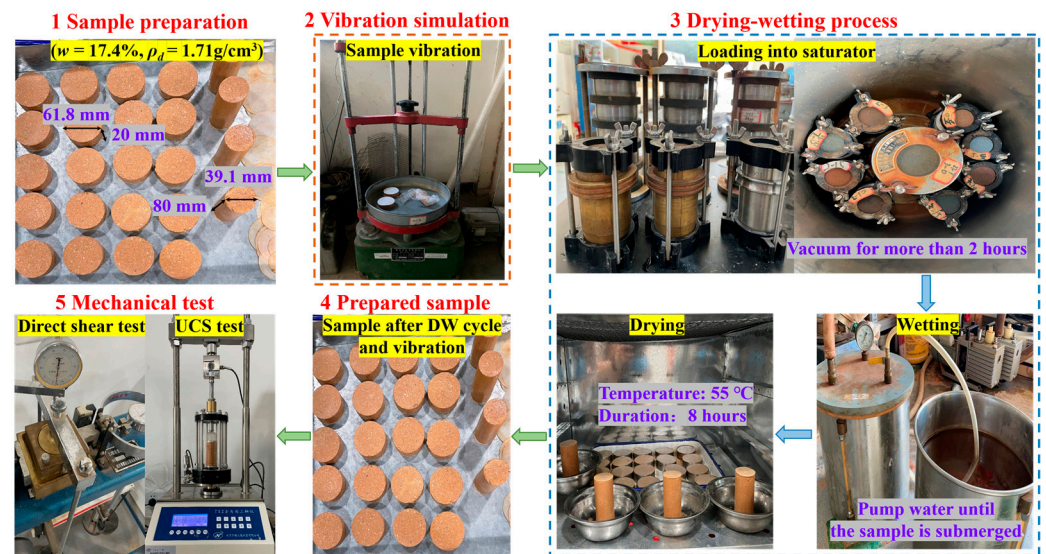


Figure 3. Experimental flowchart.

2.2.1. Sample Preparation

The GRS samples were prepared according to the specification [32]. Firstly, the retrieved soil samples were gently crushed with a rubber hammer and dried. Subsequently, a suitable amount of distilled water was added to the dried soil to achieve the same water content and dry density as the in situ soil ($w = 17.6\%$, $\rho_d = 1.71 \text{ g/cm}^3$). The mixture was then placed in a sealed bag for over 24 h to ensure uniform moisture distribution within the soil. Finally, according to the dry density and water content, the required sample soil mass is weighed. The direct shear sample was pressed into a ring cutter using static pressure through a sampler to make a sample with a diameter of 61.8 mm and a height of 20 mm; the triaxial samples were compacted in five equal layers on the bottom plate inside a split mold with a diameter of 39.1 mm and a height of 80 mm. After the samples are prepared, they need to be reweighed to ensure that the difference in quality between the samples does not exceed 1%.

2.2.2. Vibration Simulation and Drying–Wetting Cycle Process

In order to simulate the effects of mechanical vibration and hot and rainy climates on the soil samples, the specimens were first vibrated and then simulated with DW cycles.

(1) Vibration simulation

Referring to the vibration method in Refs. [27,28], a ZBSX-92A shock vibrating sieve machine was used to simulate the effect of mechanical vibration on the soil. To observe the effect of specimen disturbance on strength degradation of GRS, the duration of vibration was determined based on previous preliminary experiments. The vibration duration was different for the direct shear specimens and the UCS specimens. The former was set at 15 min, 30 min and 45 min and the latter at 5 min, 10 min and 15 min. To prevent moisture loss during vibration, the specimens were wrapped in cling film and placed on a matching vibrating sieve tray. The completion of these steps marked the end of the vibration specimen preparation process.

(2) Drying–wetting cycle process

In this study, the number of DW cycles for the tests was set to range from 0 to 5 cycles. Each DW cycle consisted of two stages: drying process and wetting process. The specific path of the DW cycle can be found in Figure 4.

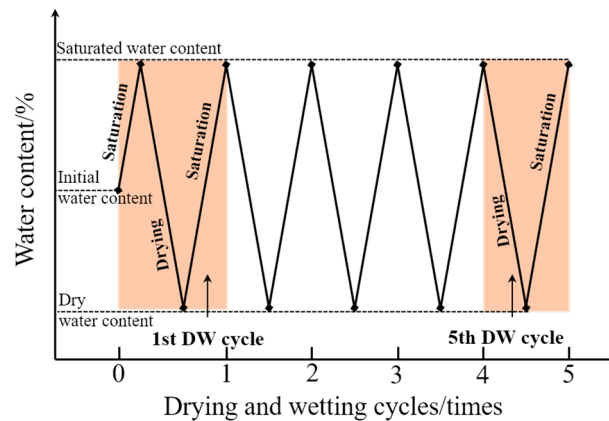


Figure 4. Sample drying and wetting cycle path.

Drying process. The soil specimens were put into the oven at 55 °C for about 8 h, then taken out and left for 24 h to naturally cool down to room temperature. When the moisture content of a specimen is maintained at about 10%, it is considered to be completely dry.

Wetting process. The unconfined compression strength specimens and direct shear specimens were placed in the triaxial saturation apparatus and the disk saturation apparatus, respectively, before being placed in the saturation chamber. Subsequently, the saturation chamber was evacuated using a vacuum pump for 2 h. Then, the water inlet valve of the saturation chamber was opened to fully submerge the specimens. Finally, the interior of the saturation chamber was connected to the atmosphere, and the specimens were left undisturbed for a minimum of 24 h to complete the saturation process.

2.2.3. Mechanical Test

The specimens that underwent vibration and DW cycle simulations were used for both direct shear tests and unconfined compression strength tests. For each test condition, two sets of control experiments were set up, and the coefficient of variation (C_v) for the same group of experiments should be less than 10%. When the $C_v < 10\%$, the average of the two is taken. If $C_v > 10\%$, the experiment needs to be reconducted until C_v meets the requirements. The specific experimental plans can be found in Table 2.

Table 2. Mechanical test program for GRS.

Test Name	Vibration Duration/min	DW Cycles /Times	Normal Load /kPa	Number of Specimens/pc
Direct shear test	0, 15, 30, 45	0, 1, 2	100, 200	288
UCS test		3, 4, 5	300, 400	
			—	72

(1) Direct shear test

The direct shear tests were conducted using consolidated quick shear on an EDJ-2 strain control direct shear apparatus. The normal stress on the specimens was set at 100 kPa, 200 kPa, 300 kPa and 400 kPa. After applying the normal stress for 5 min, water was filled into the shear box. When the vertical deformation changed less than 0.005 mm per hour, the consolidation was considered complete and the shearing process began, with a shear rate of 0.8 mm/min.

(2) Unconfined compression strength test

For the unconfined compression strength tests, a TSZ fully automatic triaxial apparatus was used. Vaseline was applied to the surface of the specimens to prevent moisture evaporation. The shear rate during the test was set at 1.2 mm/min, and the loading was stopped when the axial strain reached 20%.

3. Test Results and Analysis

3.1. Analysis of Direct Shear Test Results

3.1.1. Characteristics of Stress–Strain Curve in Direct Shear Test

The stress–strain curves of the specimens after vibration and DW cycles for the direct shear tests are shown in Figure 5. The stress–strain curves of the GRS mainly exhibit strain-hardening characteristics. At 100 kPa normal stress, with the increase in the number of DW cycles, the shape of the stress–strain curve transitions from an ideal plastic type to a weak strain-hardening type. However, the increase in vibration duration does not significantly affect the stress–strain curve shape. When the normal stress exceeds 100 kPa, with the increase in the number of DW cycles and vibration time, the stress–strain curve changes from weak strain hardening to distinct strain hardening.

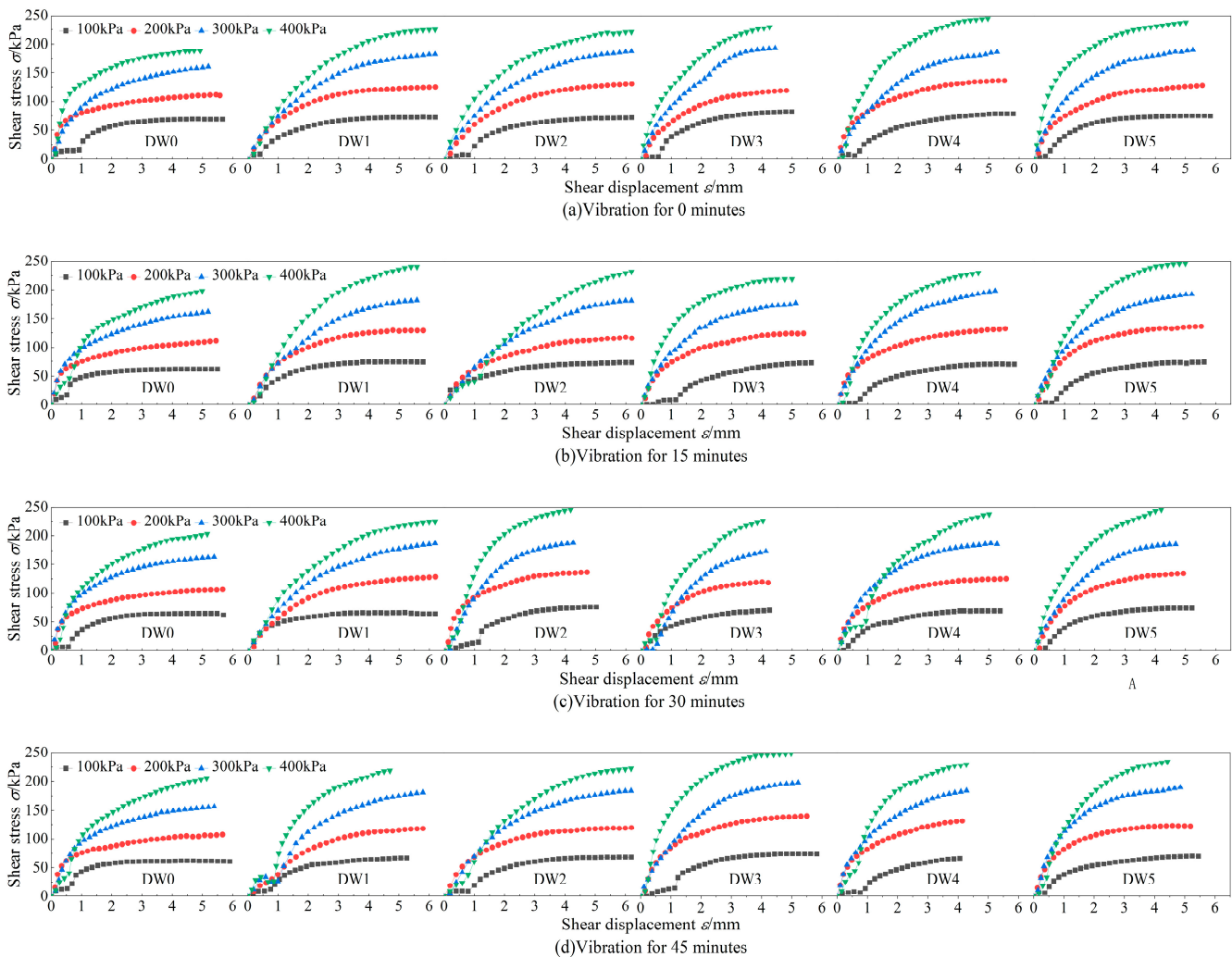


Figure 5. Stress–strain curves of direct shear test.

3.1.2. Variation in Shear Strength Parameters

(1) Cohesion

As the stress–strain curve exhibits strain hardening with no distinct peak, the shear stress corresponding to a shear displacement of 4 mm was taken as the shear strength according to the specification [32]. Based on the Mohr–Coulomb criterion, the shear strength parameters under different DW cycles and vibration times were calculated, as shown in Figure 6. The results show that the cohesion decreases nonlinearly with the increase in the number of DW cycles and vibration time. When the specimen undergoes only DW cycles or vibration, the cohesion decreases monotonically, which is in line with a study conducted

by An et al. [3]. However, when the specimen undergoes both DW cycles and vibration, the cohesion exhibits fluctuating decreases in the early stages of DW cycles. For example, under the vibration durations of 30 and 45 min, the cohesion experiencing one DW cycle was 5.1% and 7.6% higher than that of the specimens without DW cycles, respectively.

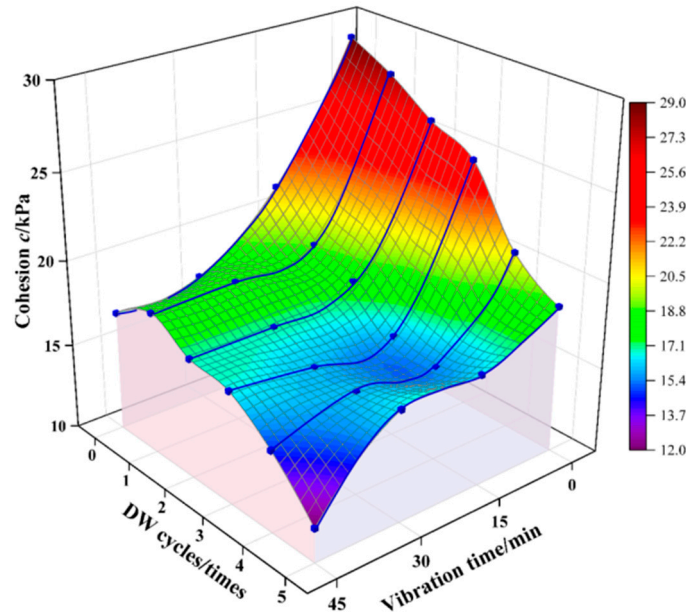


Figure 6. Cohesion change graph.

The degradation cohesion index $\zeta_{t,n}$ was used to quantify the effects of DW cycles and vibration on cohesion degradation, as defined in Equation (1), and the calculation results are presented in Table 3.

$$\zeta_{t,n} = \frac{c_{0,0} - c_{t,n}}{c_{0,0}} \times 100\% \tag{1}$$

where $\zeta_{t,n}$ is the cohesion degradation index after t minutes of vibration and n times of DW cycles; $c_{0,0}$ is the cohesion without DW cycles or vibration; and $c_{t,n}$ is the cohesion after t minutes of vibration and n times of DW cycles.

Table 3. $\zeta_{t,n}$ under DW cycles and vibration.

Vibration Time/mins	Cohesion Degradation Index $\zeta_{t,n}/\%$					
	DW Cycles/Times					
	0	1	2	3	4	5
0	0.0	4.5	10.5	14.8	30.3	35.9
15	26.2	33.1	37.9	40.3	38.8	42.6
30	39.7	36.6	40.6	44.8	44.8	43.1
45	41.4	36.9	41.4	42.8	49.1	58.6

Table 3 shows that the cohesion undergoes significant degradation when specimens are subjected to either DW cycles or vibration alone. $\zeta_{t,n}$ reaches 41.4% and 35.9% when the specimens are vibrated for 45 min or undergo five DW cycles, respectively. The degradation effect of GRS under the combined action of DW cycles and vibration is not simply additive. Under the first three DW cycles, the degradation from 0 to 15 min of vibration is remarkably significant, with a difference in $\zeta_{t,n}$ exceeding 26%. Under the last two DW cycles, the difference in $\zeta_{t,n}$ between 0 and 15 min of vibration is less than 8.5%. Under the same vibration time (except for 0 min), there is no significant degradation in $\zeta_{t,n}$ with the increase in the number of DW cycles. The average difference in $\zeta_{t,n}$ between 5 and 0 DW cycles is approximately 15%.

(2) Internal friction angle

Figure 7 presents that the internal friction angle increases in a fluctuating manner with the increase in the number of DW cycles and vibration time. The research results regarding the influence of DW cycles on the internal friction angle are inconsistent. Some scholars believe that DW cycles mainly weaken interparticle bonding, but the main factor affecting the variation in the internal friction angle is the frictional characteristics between soil particles. Therefore, the impact of DW cycles on the internal friction angle is not significant [4,14]. However, some scholars argue that the matric suction generated by DW cycles can cause consolidation and volume shrinkage of the soil, enhancing the contact between soil particles, thereby leading to an increase in the internal friction angle [34,35]. The latter view is more in line with the results of this study. During the experiment, the specimens indeed underwent significant irreversible shrinkage after DW cycles, as shown in Figure 8. The left and right images in Figure 8 depict the morphology of the specimen before and after DW cycles, respectively. Initially, the specimen occupies the entire space within the ring cutter. However, after the DW cycles, noticeable gaps form between the specimen and the ring cutter, clearly indicating that the specimen has experienced a reduction in volume due to the DW cycles, and the consolidation effect of DW cycles on the soil volume is greater than the development of internal cracks within the soil, resulting in an increase in the internal friction angle.

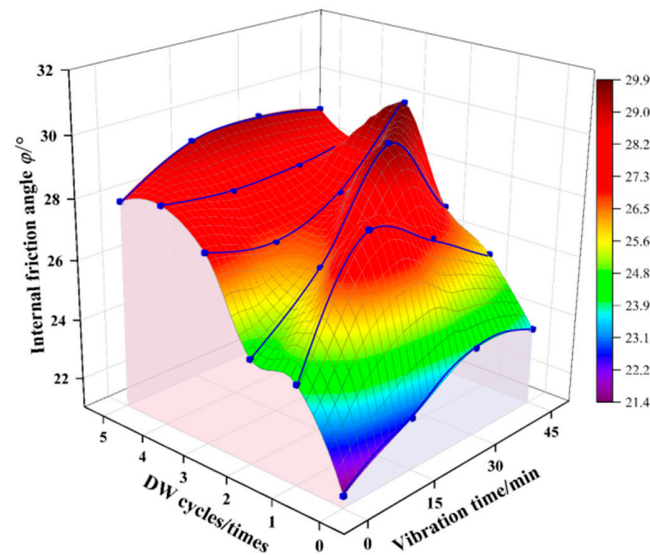


Figure 7. Angle of internal friction change graph.

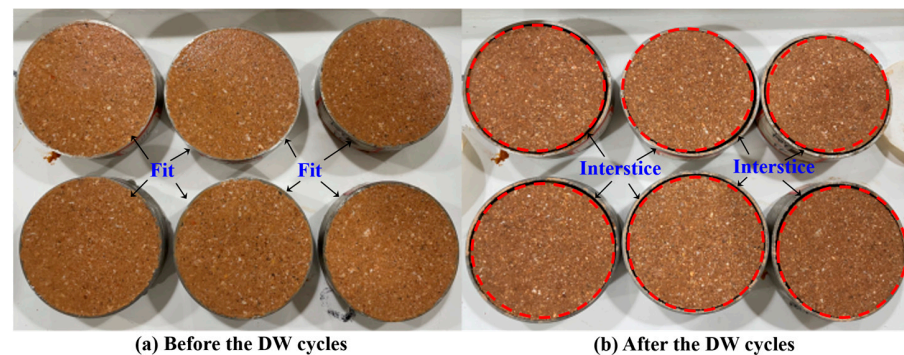


Figure 8. Specimen volume shrinkage diagram.

Compared with the effect of the DW cycle on the internal friction angle of GRS, the effect of vibration is not significant. The vibrations not only lead to closer contact between soil particles but also cause the breakup of larger particle aggregates. Therefore, the influence of vibration on the internal friction angle is not as significant as that of the

drying–wetting cycle. In addition, the effect of vibration on the internal friction angle gradually weakens with an increase in the number of DW cycles. When the number of DW cycles reaches five, the effect of vibration is almost negligible.

3.1.3. Modification of the Shear Strength Formula

The above analysis indicates that both the DW cycle and vibration have a significant influence on the cohesion and internal friction angle of GRS. Therefore, it is necessary to modify the shear strength formula.

Figure 9 shows the relationship between the cohesion degradation index $\zeta_{t,n}$ and the number of DW cycles. The relationship for unvibrated and vibrated specimens is different. When there is no vibration, $\zeta_{t,n}$ is approximately exponentially related to the DW cycle. However, when there is vibration, $\zeta_{t,n}$ is approximately linear with the number of DW cycles.

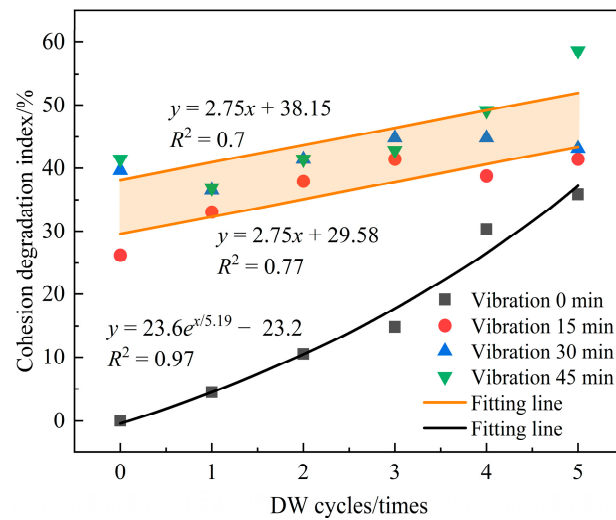


Figure 9. Cohesion degradation index vs. DW cycles.

For the purposes of nondimensionalization and applicability, let v equal $t/45$, and by substituting Equation (1) into the fitting formula, the modified formulas for cohesion under different vibration times are obtained, as shown in Equation (2).

$$c_{v,n} = \begin{cases} c_{0,0}(1.23 - 0.23e^{n/5.13}), & v = 0, 0 \leq n \leq 5 \\ c_{0,0}(0.75 - 0.03n - 0.13v), & \frac{1}{3} \leq v \leq 1, 0 \leq n \leq 5 \end{cases} \quad (2)$$

where v is the normalized vibration time, $v = t/45$, where t is the vibration time and 45 is the maximum vibration time; $c_{v,n}$ is the cohesion under n th DW cycles and the normalized vibration time v ; and $c_{0,0}$ is the initial cohesion (without DW cycles and vibration).

Figure 10 presents the relationship between the normalized internal friction angle and the number of DW cycles. The internal friction angle ratio is approximately linear with the number of DW cycles, and the correction formula for the internal friction angle is shown in Equation (3).

$$\varphi_n = \begin{cases} (0.073n + 1)\varphi_0, & v = 0, 0 \leq n \leq 5 \\ \beta(0.073n + 1)\varphi_0, & \frac{1}{3} \leq v \leq 1, 0 \leq n \leq 5 \end{cases} \quad (3)$$

where φ_n and φ_0 are the internal friction angle for the n th and initial friction angle, respectively; β is the correction factor, taking 1.1 for $0 \leq n \leq 2$ and 1.03 for $3 \leq n \leq 5$.

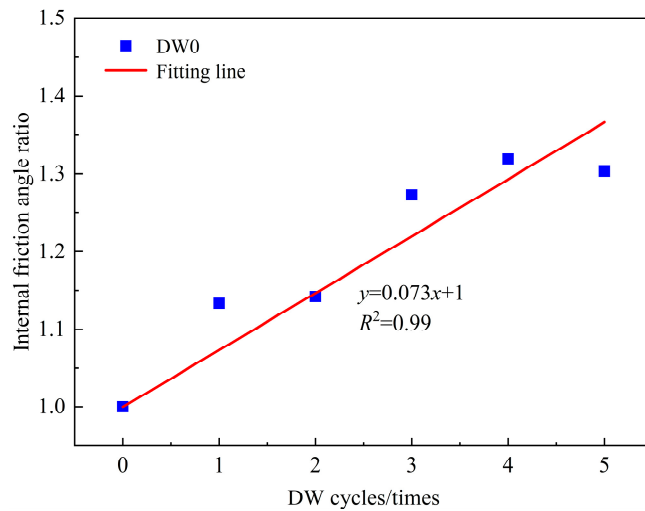


Figure 10. Internal friction angle ratio vs. DW cycle.

So, the fitting formula for shear strength can be modified as follows:

$$\tau_{v,n} = \begin{cases} \sigma \tan[(0.073n + 1)\varphi_0] + c_{0,0}(1.23 - 0.23e^{n/5.13}), & v = 0, 0 \leq n \leq 5 \\ \sigma \tan[\beta(0.073n + 1)\varphi_0] + c_{0,0}(0.75 - 0.03n - 0.13v), & \frac{1}{3} \leq v \leq 1, 0 \leq n \leq 5 \end{cases} \quad (4)$$

where $\tau_{v,n}$ is the shear strength under n th DW cycles and the normalized vibration time v ; σ is the normal stress.

Figure 11 shows a comparison of shear strength calculated using Equation (4) and the measured values for all DW cycle numbers and vibration times. The diagonal line is the contour line, where the measured values are equal to the predicted values. The data errors are all within 10%, demonstrating that the modified shear strength formula has high prediction accuracy.

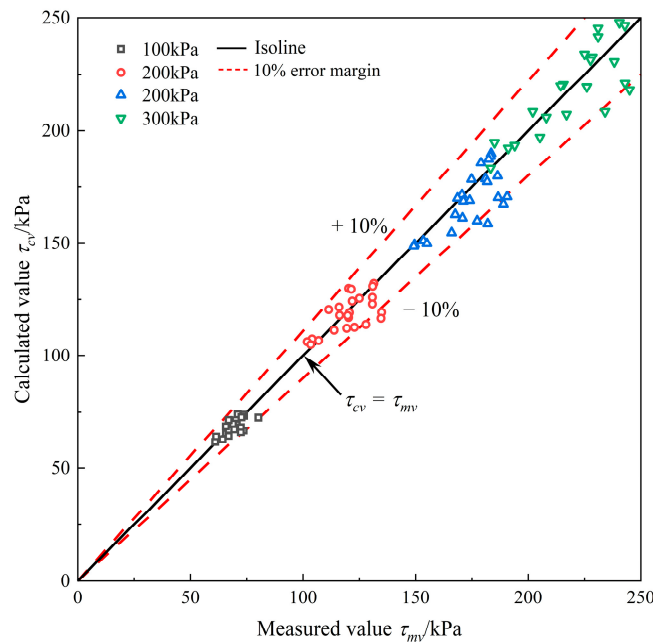


Figure 11. Comparison of measured and calculated values of shear strength.

3.2. Analysis of Unconfined Compression Strength Test Results
 3.2.1. Characteristics of Stress–Strain Curve in UCS Test

Figure 12 presents the stress–strain curve of the UCS test. Most of the stress–strain curves are strain-softening, i.e., there is a clear downward trend after reaching a peak. Additionally, the DW cycle and vibration have a significant influence on the shape of the stress–strain curve. With an increase in the number of DW cycles and vibration time, the UCS gradually decreases. The most significant change was observed after the first DW cycle or 5 min of vibration for the specimens. Compared to vibration, the DW cycle has a greater impact on the stress–strain curve. After undergoing five DW cycles, the UCS of the specimen without vibration decreases by approximately 60%, while after 15 min of vibration without DW cycles, the UCS decreases by 44%. The combination of the DW cycle and vibration causes the specimen to reach the UCS at a small axial strain. From Figure 12a,b, it can be observed that the UCS is at around 15% axial strain. From Figure 12c,d, it can be observed that after four DW cycles, the UCS shifts to before 7.5% axial strain, indicating that the coupling effect of both factors greatly deteriorates the structure of the soil specimen, leading to rapid failure of the soil specimen under compression.

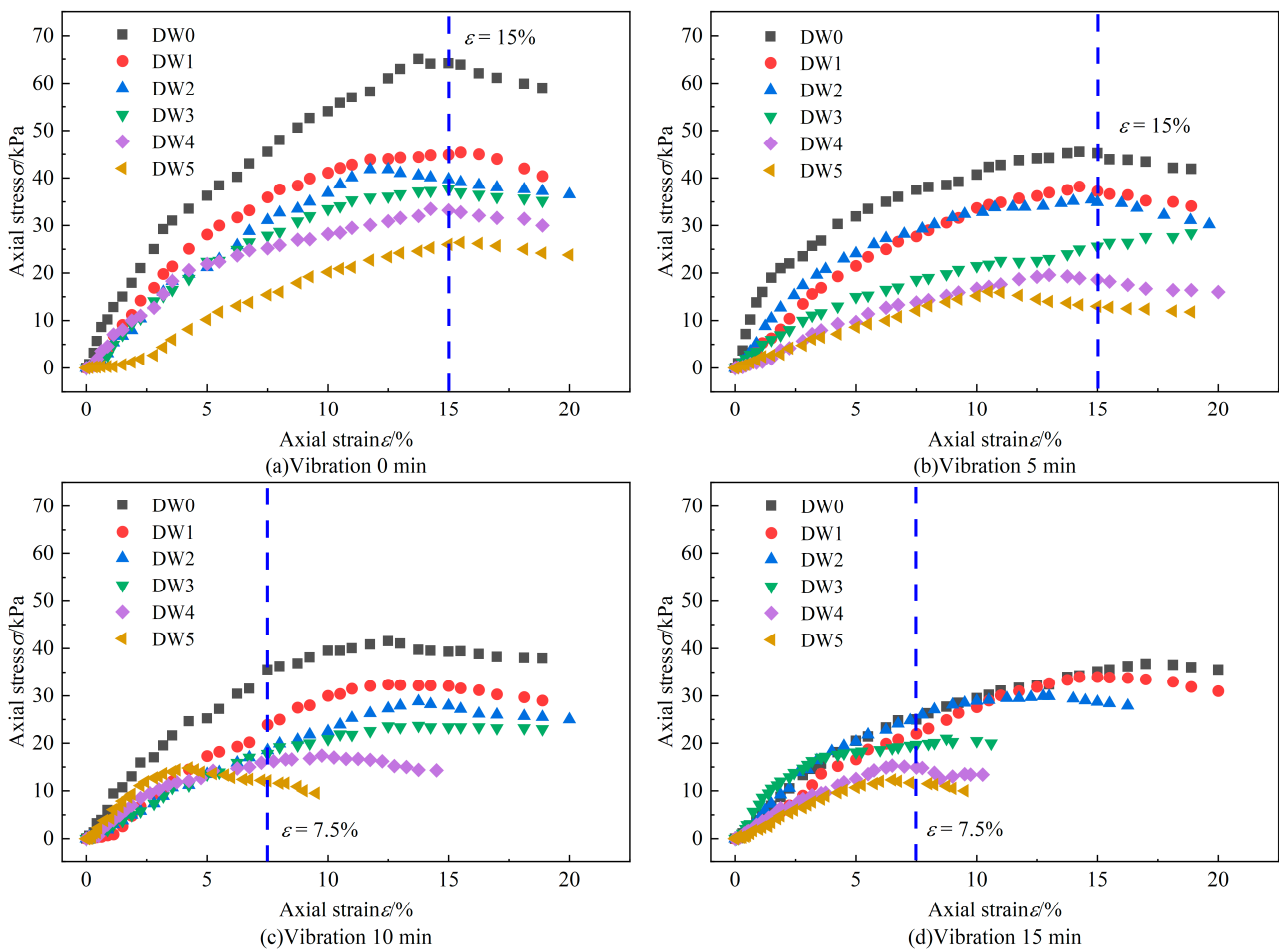


Figure 12. Stress–strain curve of unconfined compression strength test.

3.2.2. Unconfined Compression Strength

Figure 13 shows the relationship between UCS and the number of DW cycles and vibration time. The UCS decreases rapidly with an increase in the number of DW cycles and vibration time, the rate of decrease gradually slows down and eventually stabilizes and the trend of changes caused by vibration time is similar to that of Liu et al. [29].

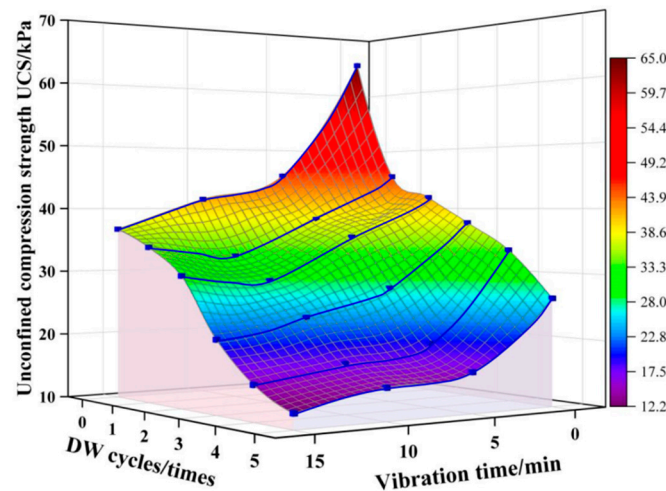


Figure 13. Unconfined compression strength change graph.

To further quantify the effect of DW cycles and vibration on the UCS, the degradation of UCS is calculated using Equation (5).

$$\eta_{t,n} = \frac{UCS_{0,0} - UCS_{t,n}}{UCS_{0,0}} \times 100\% \tag{5}$$

where $\eta_{t,n}$ is the UCS degradation index after t minutes of vibration and n th DW cycles; $UCS_{0,0}$ is the UCS without DW cycles and vibration; and $UCS_{t,n}$ is the UCS after t minutes of vibration and n th DW cycles.

The calculation results of $\eta_{t,n}$ are shown in Table 4. It can be observed that the DW cycle and vibration have a significant degradation effect on the UCS, reaching a maximum of 81.1%. The initial DW cycles and vibration have the most significant impact, with $\eta_{t,n}$ reaching 30.2% and 30%, respectively. When the vibration time increases from 5 min to 15 min, there is little change in $\eta_{t,n}$, with an average increase of about 10%.

Table 4. $\eta_{t,n}$ under DW cycles and vibrations.

Vibration Time/mins	UCS Degradation Index $\eta_{t,n}/\%$					
	DW Cycles/Times					
	0	1	2	3	4	5
0	0.0	30.2	35.7	42.0	48.5	59.4
5	30.0	41.2	45.5	57.5	69.8	75.2
10	36.2	50.2	55.7	63.7	73.2	77.2
15	43.5	47.7	54.0	67.7	76.5	81.1

Figure 14 presents the relationship between the UCS degradation index $\eta_{t,n}$ and the DW cycle. The relationship is nonlinear for unvibrated specimens, while it is approximately linear for vibrated specimens. By substituting Equation (5) into the fitting formula, the USC under DW cycles and vibrations can be obtained, as shown in Equation (6).

$$UCS_{v,n} = \begin{cases} UCS_{0,0}(1 - 0.27n^{0.45}), & v = 0 \\ UCS_{0,0}(0.74 - 0.1n + 0.045nv - 0.45v), & \frac{1}{3} \leq v \leq 1 \end{cases} \tag{6}$$

where v is the normalized vibration time, $v = t/15$, where t is the vibration time, and 15 is the maximum vibration time; $UCS_{v,n}$ is the UCS under n th DW cycles and the normalized vibration time v .

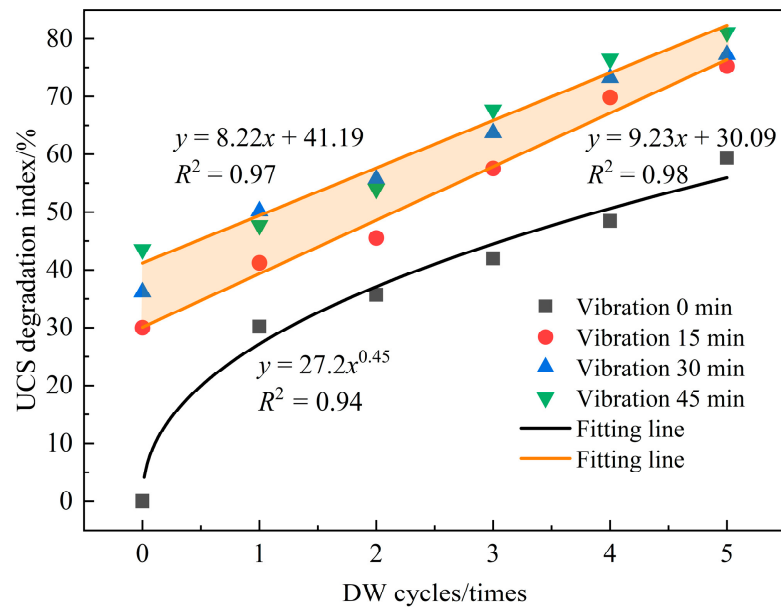


Figure 14. UCS degradation index vs. DW cycle.

Figure 15 shows a UCS comparison of the calculated and measured values for different vibration times under 0–5 DW cycles. The diagonal line is the contour line, where the measured values are equal to the predicted values. The data errors are all within 8%, indicating that the modified UCS formula has good accuracy.

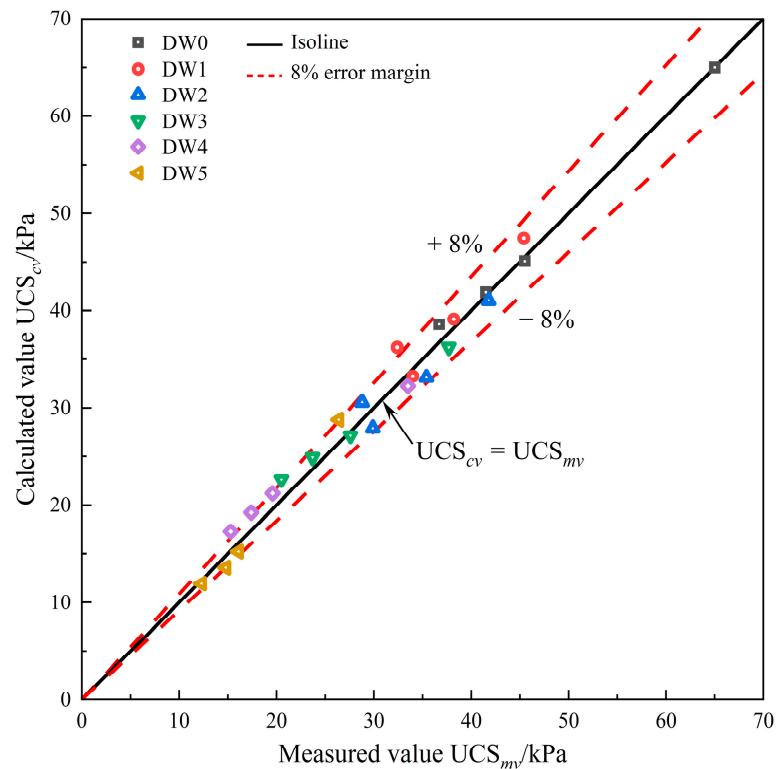


Figure 15. Comparison of measured and calculated values of UCS.

4. Conclusions

Through direct shear and UCS tests, the stress–strain curves, cohesion, internal friction angle and UCS of GRS were studied. Modified calculation formulas for shear strength and unconfined compression strength under DW cycles and vibration were proposed. The

proposed modified formulas enable the use of more accurate GRS mechanical parameters in numerical simulations, as opposed to the outdated parameters often found in geotechnical survey reports. Furthermore, the research provides specific mechanical parameter changes for considering soil in different influencing areas, such as areas affected only by DW cycles, areas affected only by vibrations and areas where the two factors intersect. By applying more precise grid mechanical parameters to these distinguishing regions, researchers can obtain more accurate simulation results. The following conclusions were drawn:

- (1) The stress–strain curve of shear strength mainly exhibited strain-hardening characteristics. Due to the volume shrinkage caused by DW cycles and vibration, the shear compressibility of the sample increased with the number of DW cycles and the vibration time. The stress–strain curve of unconfined compression strength showed strain-softening characteristics, with a significant decrease in the stress peak due to DW cycles and vibration, and their combined effect shifted the stress peak forward in the stress–strain curve.
- (2) The cohesion decreased nonlinearly with the increase in the number of DW cycles and the vibration time, and the degradation of cohesion reached 58.6% under their combined effect, but the degradation effect was not simply additive. The compaction effect of DW cycles on the soil caused a fluctuating increase in the internal friction angle with the increase in the number of DW cycles. The influence of vibration on the internal friction angle decreased with the increase in the number of DW cycles.
- (3) The UCS rapidly decreased and then stabilized with the increase in the number of DW cycles and vibration time. The degradation effect of UCS due to DW cycles and vibration was significant, with a maximum degradation of 81.1%. Without vibration, the degradation of UCS increased nonlinearly with the number of DW cycles, while after experiencing vibration, the degradation of UCS increased linearly with the number of DW cycles.
- (4) Modified formulas considering the effects of DW cycles and vibration on shear strength and UCS were established. The calculated values of the two modified formulas were within a reasonable range of error compared to the measured values, indicating that the modified formulas can effectively predict the effects of DW cycles and vibration on shear strength and UCS.

Author Contributions: Investigation, D.C.; data curation, J.T.; writing—original draft, J.T.; writing—review and editing, D.C.; supervision, D.C.; project administration, D.C. All authors have read and agreed to the published version of the manuscript.

Funding: The work in this paper was supported by the Natural Science Foundation of Fujian Province (No.: 2021J01010), the Key Program of Natural Science Foundation of Fujian Province (No.: 2021J02003) and China Railway Southern Group 2022 Science and Technology Innovation Program Topics (No.: 202208).

Institutional Review Board Statement: Not applicable.

Informed Consent Statement: Not applicable.

Data Availability Statement: The data are available and are explained in this article; readers can access the data supporting the conclusions of this study.

Conflicts of Interest: The authors declare no conflicts of interest.

References

1. Wang, T.H.; Dai, J.; Shui, W.H. *Research on the Deformation Calculation Method for Settlement of Residual Soil Foundation*; China Architecture & Building Press: Beijing, China, 2011.
2. Wang, G.; Zhang, X.W.; Liu, X.Y.; Xu, Y.Q.; Lu, J.F. Microscopic evolution of pore characteristics and particle orientation of granite residual soil in one-dimensional compression. *Geofluids* **2022**, *2022*, 8380656. [[CrossRef](#)]
3. An, R.; Kong, L.W.; Li, C.S.; Luo, X.Q. Strength attenuation and microstructure damage of granite residual soils under hot and rainy weather. *Chin. J. Rock Mech. Eng.* **2020**, *39*, 1902–1911. [[CrossRef](#)]

4. An, R.; Zhang, X.W.; Kong, L.W.; Liu, X.Y.; Chen, C. Drying-wetting impacts on granite residual soil: A multi-scale study from macroscopic to microscopic investigations. *Bull. Eng. Geol. Environ.* **2022**, *81*, 447. [CrossRef]
5. Wang, H.B.; Zhou, Y.; Yu, G.; Zhou, B.; Zhang, A.-J. A triaxial test study on structural granite residual soil. *Rock Soil Mech.* **2021**, *42*, 991–1002.
6. Zhou, X.W.; Liu, P.; Hu, L.M.; He, Y.B.; Zhao, S. An experimental study of shear yield characteristics of structured granite residual soil. *Rock Soil Mech.* **2015**, *36*, 157–163.
7. Tang, L.S.; Sang, H.T.; Song, J.; Liu, F.T.; Yan, B.; Zhang, P.C. Research on soil particle joint function and brittle-elastoplastic cement damage model of unsaturated granite residual soil. *Rock Soil Mech.* **2013**, *34*, 2877–2888.
8. An, R.; Li, C.S.; Kong, L.W.; Guo, A.-G. Effects of drilling disturbance and unloading lag on in-situ mechanical characteristics of granite residual soil. *Chin. J. Geotech. Eng.* **2020**, *42*, 109–116.
9. Shu, R.J.; Kong, L.W.; Wang, J.T.; Jian, T.; Zhou, Z.-H. Mechanical behavior of granite residual soil during wetting considering effects of initial unloading. *Chin. J. Geotech. Eng.* **2022**, *44*, 154–159+165.
10. Chen, D.X.; Tang, J.R.; Yang, X.F. Effects of drying-wetting cycle and fines content on hysteresis and dynamic properties of granite residual soil under cyclic loading. *Appl. Sci.* **2023**, *13*, 6660. [CrossRef]
11. Yang, X.F.; Chen, D.X.; Liu, Y. Crack development and slope stability of granite residual soil under dry-wet cycles. *J. Xiamen Univ. (Nat. Sci.)* **2022**, *61*, 591–599.
12. Yin, S.; Kong, L.W.; Zhang, X.W. Experimental study on stiffness characteristics of residual soil at small strain under hot and rainy climate. *Chin. J. Geotech. Eng.* **2017**, *39*, 743–751.
13. Jian, W.B.; Hu, H.R.; Luo, Y.H.; Tang, W.Y. Experimental study on deterioration of granite residual soil strength in wetting-drying cycles. *J. Eng. Geol.* **2017**, *25*, 592–597.
14. Yu, J.J.; Chen, D.X.; Wang, H.; Zhang, B. Analysis of the shear strength of granite residual soil and slope stability under wetting-drying cycles. *J. Xiamen Univ. (Nat. Sci.)* **2019**, *58*, 614–620.
15. Liu, P.; Chen, R.P.; Wu, K.; Kang, X. Effects of drying-wetting cycles on the mechanical behavior of reconstituted granite-residual soils. *J. Mater. Civ. Eng.* **2020**, *32*, 04020199. [CrossRef]
16. Liu, Y.; Chen, D.X.; Wang, H.; Yu, J.J. Response analysis of residual soil slope considering crack development under drying-wetting cycles. *Rock Soil Mech.* **2021**, *42*, 1933–1943+1982.
17. An, R.; Kong, L.W.; Zhang, X.W.; Guo, A.G.; Bai, W. A multi-scale study on structure damage of granite residual soil under wetting-drying environments. *Chin. J. Rock Mech. Eng.* **2023**, *42*, 758–767.
18. An, R.; Kong, L.W.; Zhang, X.W.; Guo, A.; Bai, W.; Singh, D.N. Weathering degree effects on strength indexes of residual soil based on in-situ borehole shear tests. *J. Basic Sci. Eng.* **2022**, *30*, 1275–1286.
19. Hu, Q.; Xu, S.F.; Chen, R.P.; Long, R. Influence of soil disturbance on metro tunnel in soft clay due to excavation of deep foundation pit. *Chin. J. Geotech. Eng.* **2013**, *35*, 537–541.
20. Shen, S.L.; Tang, C.P.; Pang, X.M. Disturbance and strength recovery of surrounding clays around soil-cement columns installed by different mixing methods. *Rock Soil Mech.* **2006**, 1827–1830. [CrossRef]
21. Chen, Y.M.; Hu, Q.; Chen, R.P. Soil disturbance by the collapse of retaining wall for a pit excavation and the induced additional settlement: A case study of Hangzhou Metro Xianghu Station. *China Civ. Eng. J.* **2014**, *47*, 110–117.
22. Gomes, R.C. Effect of stress disturbance induced by construction on the seismic response of shallow bored tunnels. *Comput. Geotech.* **2013**, *49*, 338–351. [CrossRef]
23. Deng, Y.F.; Liu, S.Y. Effect of sample disturbance on soft soil strength. *Chin. J. Rock Mech. Eng.* **2007**, 1940–1944. Available online: <https://kns.cnki.net/kcms2/article/abstract?v=vs6GoGUiQCOBModo75s4TXHmDPfM4uDQ9oFScd7csBOcteNiO9xSxrlsTDyR0I5eW700gIdDq78nHRqKBvxl8haAhMaxJM-HDNBIRfWZPSC0MiOC0P-AbkiljyHOGAae7m7oTDXAr8=&uniplatform=NZKPT&language=CHS> (accessed on 1 December 2023).
24. Chen, H.; Ma, K.S. Study on effect of moisture to strength recovery of disturbed silt. *Sci. Technol. Eng.* **2015**, *15*, 184–188.
25. Bai, S.Y.; Wang, W.J.; Xie, X.Y.; Zhu, D.-L. Experimental study on HS-small model parameters of soil considering disturbance and its application in foundation pit engineering. *Rock Soil Mech.* **2023**, *44*, 206–216.
26. Zhou, Y.M.; Deng, Z.W.; Fan, Z.J.; Liu, W.J. Shear strength deterioration of compacted residual soils under a wind turbine due to drying-wetting cycles and vibrations. *Adv. Civ. Eng.* **2021**, *2021*, 8628842. [CrossRef]
27. Du, W.B.; Huang, B.; Wang, M.Y.; Lu, J.Z.; Zheng, Y.D. Influence of salinity on mechanical properties of marine clay and pre-consolidation test of disturbance. *Yangtze River* **2020**, *51*, 189–193.
28. Liu, J.H. Study on Deformation of Granite Residual Soil Foundation Pit Considering Disturbance and Water Content Change. Master's Thesis, Fuzhou University, Fuzhou, China, 2020.
29. Liu, J.J.; Zeng, G.H.; Meng, L.S.; He, W.B. Study on the effect of disturbance on the thixotropic strength increasing of silt. *Chin. J. Undergr. Space Eng.* **2016**, *12*, 1294–1299.
30. Liu, G.Y.; Yang, S.S.; Wang, Y.P.; Yu, Y. Study on effect of moisture to strength recovery of disturbed silt. *Sichuan Build. Sci.* **2016**, *42*, 51–55.
31. Liu, J.M.; Qiu, Y.; Guo, T.T.; Song, W.Z.; Gu, C. Comparative experimental study on static shear strength and postcyclic strength of saturated silty clay. *Rock Soil Mech.* **2020**, *41*, 773–780.
32. GB/T50123—2019; Standard for Geotechnical Testing Method. Ministry of Water Resources of the People's Republic of China: Beijing, China, 2019.

33. DBJ-15-31-2016; Design code for building foundation. Department of Housing and Urban-Rural Development of Guangdong: Beijing, China, 2016.
34. Wang, Y.; Xue, Q.; Wu, Y.; Zhao, L.Y. Mechanical properties and micromechanisms of compacted clay during drying-wetting cycles. *Rock Soil Mech.* **2015**, *36*, 2815–2824.
35. Tu, Y.L.; Liu, X.R.; Zhong, Z.L.; Wang, S.; Wang, Z.J.; Ke, W. Experimental study on strength and deformation characteristics of silty clay during wetting-drying cycles. *Rock Soil Mech.* **2017**, *38*, 3581–3589.

Disclaimer/Publisher’s Note: The statements, opinions and data contained in all publications are solely those of the individual author(s) and contributor(s) and not of MDPI and/or the editor(s). MDPI and/or the editor(s) disclaim responsibility for any injury to people or property resulting from any ideas, methods, instructions or products referred to in the content.